Localization of high-energy electron scattering from atomic vibrations

C. Dwyer[*]

Ernst Ruska-Centre for Microscopy and Spectroscopy with Electrons and Peter Grünberg Institute,
Forschungszentrum Jülich, D-52425 Jülich, Germany

Electrons with kinetic energies ∼100 keV are potentially capable of exciting atomic vibrational states from a distance of microns. Despite such a large interaction distance, our detailed calculations show that the scattering physics permits a high-energy electron beam in a scanning transmission electron microscope to locate vibrational excitations with atomic-scale spatial resolution. Attempts to realize this capability experimentally could potentially benefit numerous fields across the physical sciences.

PACS number(s): 79.20.Uv, 68.37.Ma

I. INTRODUCTION

Substantial interest currently surrounds the question of whether it is possible, from the perspective of scattering physics, to use high-energy electrons to locate atomic vibrations with a spatial resolution at, or near, the atomic scale. This interest is triggered by recent reports that it may soon be possible to use an atomic-sized beam in a scanning transmission electron microscope (STEM) to perform spectroscopy at energy resolutions of the order 10 meV [1], enabling access to vibrational excitations in a transmission geometry. The ability to detect atomic vibrations with high spatial resolution would offer substantial advantages in a number of technologically important fields, such as catalysis. However, its feasibility has been questioned due to the large degree of "inelastic delocalization," which measures the distance from which a passing electron can induce an excitation [2,3]. For a 100 keV electron (typical for a STEM), the delocalization length for vibrational excitations is 1–10 μm, i.e., *far* greater than the size of an atom or molecule, which might imply that high spatial resolution is impossible. In fact, the delocalization for *low*-energy electrons agrees well with the accepted interaction distance [4]. On the other hand, *high-angle* scattering from atomic vibrations in the STEM is well known to give rise to atomic resolution images, but the implications are inconclusive regarding the more relevant lower-angle scattering, not least because current theories of vibrational scattering in the STEM do not include the all-important low-angle dipole scattering.

In this work, we demonstrate conclusively that high spatial resolution of vibrational excitations *is* permitted by the scattering physics. We demonstrate this via explicit calculations of vibrational-loss STEM images of selected molecules based on a quantum theory of inelastic electron scattering *that includes the dipole scattering*. We find that, while delocalization effects can be significant, they do not necessarily preclude atomic spatial resolution. The interpretation of the image contrast, however, can be nontrivial. These results will be of central importance to the development of high-spatial-resolution vibrational spectroscopy as an analytical technique in the physical sciences.

II. BACKGROUND

High-spatial-resolution electron-energy-loss spectroscopy (EELS) in the STEM has become an extremely powerful tool for the analysis of materials. In this technique, an energy-loss spectrum is acquired for each position of the electron beam. The signal from inelastic scattering processes of interest is extracted from each spectrum (by subtracting any other "background" signals) and plotted as a function of beam position to form an image. In the case of core-level excitations, this technique enables mapping of a material's chemical composition and electronic bonding at the atomic scale [5–7], which is ideal for studying interfaces and nanomaterials, for example. In terms of the scattering physics, this spatial resolution is permitted first by the atomic-sized beam, and second by the inelastic delocalization length v/ω (where v is the electron's velocity and $\hbar\omega$ is the energy loss), which is typically a few angstroms or less for core-level excitations.

On the other hand, using incident electrons to access vibrational excitations presently requires techniques such as high-resolution EELS (HREELS), which uses low incident energies (a few eV) in a reflection geometry [4,8]. The superior energy resolution of this technique can reveal vibrational excitations as sharp peaks in the spectra, at energy losses corresponding to vibrational transitions. HREELS has proven to be extremely powerful in studies of adsorbate molecules on surfaces, for example, where it has enabled fundamental advances in our understanding of molecule-surface interactions. However, the spatial resolution of HREELS is limited, falling well short of the atomic scale.

The benefits of combining atomic-spatial and vibrational-energy resolutions could potentially enable fundamental advances in numerous fields. To assess the spatial resolution afforded by the physics, we have used a quantum theory of inelastic electron scattering to calculate vibrational EELS images of selected molecules assuming a STEM-EELS geometry.

III. THEORY

We employ a quantum theory of molecular vibrations in the harmonic approximation. We use the molecular properties calculated by density functional theory under the pseudopotential and generalized-gradient approximations [9,10]. Molecular vibrational properties were computed using the "finite displacements" method [11,12], assuming a temperature of 300 K.

---

*c.dwyer@fz-juelich.de

To calculate the inelastic electron scattering, we use a multislice solution to Yoshioka's equations for dynamic elastic and inelastic scattering [13]. Such a theory employs the paraxial approximation, valid for high-energy electrons. Here, the nature of the targets (described below) mean that elastic scattering has negligible consequences, and it was therefore omitted.

A key quantity in our discussion is the two-dimensional Møller potential for creating one additional quantum in vibrational mode ν in the target, given by

$$V_\nu(x,y) = \int_{-\infty}^{\infty} dz \, \langle n_\nu + 1 | \hat{V}(\mathbf{r}) | n_\nu \rangle e^{-i(\omega_\nu/v)z}$$
$$= \left(\frac{\hbar(n_\nu + 1)}{2\omega_\nu} \right)^{1/2} \sum_\kappa \frac{\mathbf{e}_\nu(\kappa)}{m_\kappa^{1/2}} \cdot \nabla_\kappa V(x,y), \tag{1}$$

where $|n_\nu\rangle$ is a vibrational state containing n_ν quanta in mode ν, $\hat{V}(\mathbf{r})$ is the Coulomb interaction energy for an electron at position $\mathbf{r}$, $\hbar\omega_\nu$ is the energy loss, the z axis coincides with the beam direction, κ labels the atoms, $\mathbf{e}_\nu(\kappa)$ is a polarization vector, m_κ is an atomic mass, and $\nabla_\kappa V(x,y)$ is the gradient of the projected electrostatic potential energy with respect to the equilibrium position of the nucleus of atom κ. Loosely speaking, $V_\nu(x,y)$ is the potential that an incident electron "sees" when it excites the vibrational mode ν. Below we refer to $V_\nu(x,y)$ simply as "the Møller potential." The effects of finite temperature are included simply by using the thermally averaged expressions for n_ν and $V(x,y)$ in the second line of Eq. (1). [A similar expression to Eq. (1) is derived in Ref. [14] for the case where the electrostatic potential is approximated by a sum of isolated-atom potentials. However, such an approximation is not used here, since it prohibits consideration of the dipole scattering.]

In the plane of the target, the wave function of an inelastically scattered electron which excites mode ν is given by

$$\psi_\nu(x,y;x_0,y_0) = -\frac{2\pi i}{\hbar v} V_\nu(x,y) \psi_0(x - x_0, y - y_0), \tag{2}$$

where $\psi_0(x,y)$ is the wave function of the incident electron beam, and (x_0,y_0) is the beam position [13]. The image intensity obtained for a beam position (x_0,y_0) is given by integrating the inelastic intensity falling within the spectrometer's entrance aperture in the far field:

$$I(x_0,y_0) = \int_{-\infty}^{\infty} du \int_{-\infty}^{\infty} dv \, D(u,v) |\tilde{\psi}_\nu(u,v;x_0,y_0)|^2, \tag{3}$$

where $\tilde{\psi}_\nu(u,v;x_0,y_0)$ is the Fourier transform of $\psi_\nu(x,y;x_0,y_0)$, and $D(u,v)$ is the detector function which equals unity for positions in the far field inside the entrance aperture and equals zero otherwise.

IV. RESULTS

We assume a STEM-EELS geometry, whereby the incident electrons form a focused coherent beam, and the images are assumed to be generated by extracting the vibrational signals in analogy with the description in Sec. II. A 100 keV beam with a convergence semiangle of 30 mrad is assumed, as appropriate for a state-of-the-art STEM equipped with aberration-corrected beam-forming optics. Such a beam is capable of 0.7 Å spatial resolution. However, in addition to the scattering mechanism itself, the actual spatial resolution achieved is also influenced by the spectrometer's collection angle [15], and so we have considered three collection angles in what follows. Our consideration of the collection angle also has practical implications, in that experimentally this angle influences the spectrometer's energy resolution.

We use multislice calculations based on fast Fourier transform with a maximum scattering angle of 316 mrad. The impact potentials (defined later) are derived from the atomic electron scattering factors of Ref. [16]. Elastic scattering has negligible consequences here and was omitted.

As targets we consider molecular H_2 and CO. The simplicity and small size of these molecules allow us to discuss spatial resolution in a straightforward context, and they are exemplary of molecules with and without an electric dipole moment, which has implications that will be made clear below. Moreover, the conclusions we draw will have relevance to potential applications of vibrational EELS imaging in catalysis.

A. Example 1: H_2 molecule

We consider a H_2 molecule, which we fix fictitiously in free space. This molecule has a bond length calculated to be 0.749 Å (the experimental value is 0.750 Å), and a vibrational stretching mode of calculated energy $\hbar\omega_{str} = 529$ meV (experiment: 517 meV [17]).

Figure 1 shows calculated vibrational EELS images of a H_2 molecule lying perpendicular to the electron beam. The Møller potential for excitation of the H_2 stretching mode [Fig. 1(a)] is related to a spatial gradient of the electrostatic potential [see Eq. (1)]. As a result, the Møller potential reverses sign at positions which are very close to the equilibrium H positions (where there is a peak in the electrostatic potential). Crucial to our assessment of spatial resolution, we see that, despite a delocalization length of $v/\omega \sim 0.2$ μm, the Møller potential is contained within an area approximately 2×2 Å^2. Therefore we immediately anticipate that the vibrational EELS images [Figs. 1(b)–1(d)] should be capable of exhibiting atomic spatial resolution, as indeed they do: For a detector semiangle $\beta = 5$ mrad, the vibrational image contains a maximum between the H atoms which, in principle, could be used to locate the position of the H_2 molecule with a spatial precision of at least 1 Å. However, the image intensity is very weak and would be difficult to observe in practice (reducing the convergence angle would increase the normalized intensity at the cost of spatial resolution). Moreover, this vibrational image also contains two strong secondary maxima (three maxima in total), as well as nonintuitive minima close to the equilibrium atomic positions which result from the zeros of the Møller potential. When β is increased to 30 mrad, these minima weaken. For $\beta = 80$ mrad the H_2 molecule appears as a more intuitive "dumbbell" shape with a shallow minimum at the center. Such behavior, where atomic-resolution STEM images are easier to interpret if the detector angle is larger than the convergence angle (here 30 mrad), is encountered in other STEM imaging modalities too; for example, bright-field
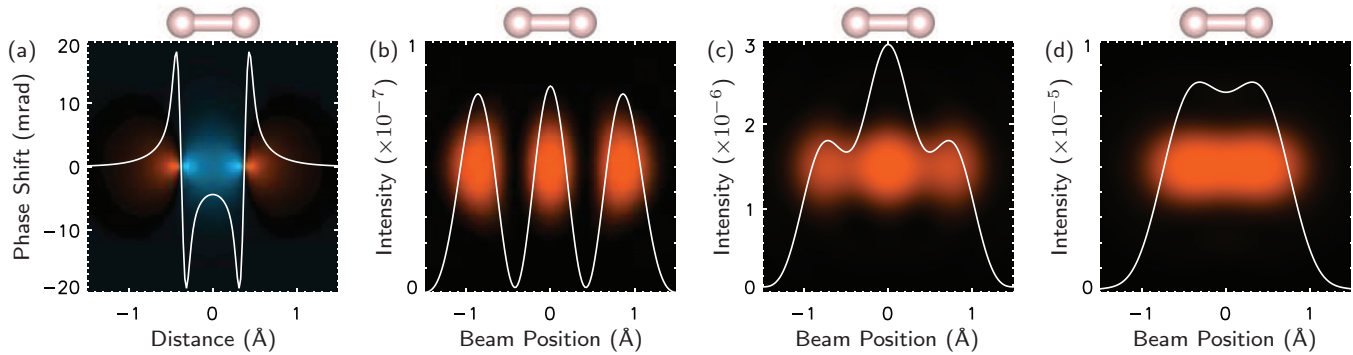
FIG. 1. (Color online) Calculated vibrational EELS images of a H_2 molecule with its molecular axis lying perpendicular to the electron beam: (a) Møller potential for excitation of the H_2 stretching mode; (b)–(d) vibrational EELS images for detector semiangles 5, 30, and 80 mrad, respectively. Each subfigure shows a square area of size indicated by the abscissa values with the H_2 molecule at the center, while the graphs show line traces along the molecular axis. The units in (a) correspond to the phase shift that would be experienced by a 100 keV incident plane wave, and the square of this phase is a measure of scattering probability. Images (b)–(d) assume an aberation-free 100 keV beam with a 0.7 Å crossover, and the intensity is normalized with respect to the incident beam intensity.

imaging [18] and core-level EELS imaging [19,20]. For $\beta = 80$ mrad the peak intensity is comparable to that obtained in core-level EELS from a single oxygen atom using a 100 eV window positioned immediately after the O K onset.

B. Example 2: CO molecule

The inversion symmetry of the H_2 molecule considered in the previous example precludes a very important consideration: A free H_2 molecule has no electric dipole moment. (H_2 does have an electric quadrupole moment, which is included in Fig. 1, although it has negligible effect.) On the other hand, many molecules possess electric dipole moments arising from the redistribution of charge that takes place during bond formation. Excitation of a vibrational mode will cause the molecule's dipole field to oscillate with period ω_v, giving rise to inelastic scattering. Here, the most important point is that the dipole fields are long ranged, extending over distances much larger than the molecules we are considering. Hence dipole scattering potentially precludes atomic spatial resolution.

We split the Møller potential into two parts: The first part, called the "impact potential," arises from changes, due to vibrations, of the molecular charge distribution that would result when electronic bonding is "switched off." The impact potential is derived from the atomic potentials, and it decays exponentially at large distances so that the scattering from it is inherently localized. The second part of the Møller potential, called the "dipole potential," arises from changes, due to vibrations, of the so-called "bonding charge." The dipole potentials were calculated by applying the Born-Oppenheimer approximation to the all-electron bonding charge density predicted by density functional theory. The names of these potentials connect with the existing literature on HREELS [4,21]. However, by our definition, the dipole potentials also contain the effects of quadrupole and higher-order moments. Furthermore, while in conventional HREELS it is unnecessary to consider the atomic-scale structure of the target when calculating dipole scattering, here it is important.

We consider a CO molecule fixed in free space. This molecule has a calculated bond length of 1.142 Å (experiment:

1.128 Å) and a single stretching mode of calculated energy $\hbar\omega_{str} = 265$ meV (experiment: 267 meV [22]). The permanent electric dipole moment was calculated to be 0.143 Debye (experiment: 0.112 D [23]). While the permanent dipole of CO is relatively small compared to that of other diatomic molecules, we find that its *dynamic* dipole (due to vibrations) is comparable to that of diatomic molecules with permanent dipoles that are one order of magnitude larger.

Figure 2 shows the effects of dipole scattering on the vibrational EELS images of a CO molecule lying perpendicular to the electron beam. As in the H_2 example above, the impact potential for excitation of the CO stretching mode [Fig. 2(a), solid line] has zeros at the equilibrium C and O positions. In contrast, the dipole potential [Fig. 2(a), dashed line, and Fig. 2(e)] has a large antisymmetric component. It is evident from Fig. 2(e) that the dipole potential extends far beyond the molecule. However, its amplitude is much smaller than that of the impact potential. In the vibrational EELS images [Figs. 2(b)–2(d)], the dipole scattering can introduce considerable asymmetry. For $\beta = 5$ mrad, where the dipole scattering makes a significant overall contribution, the effect is such that the CO molecule appears as a dumbbell displaced from its true position. This effect can be interpreted as arising from the quantum interference of impact and dipole scattering. The apparent displacement of the molecule persists for $\beta = 30$ mrad. For $\beta = 80$ mrad, dipole scattering produces only a minor effect, and now the dumbbell closely coincides with the molecule's true position. Crucially, the vibrational EELS images in Figs. 2(b)–2(d) exhibit atomic resolution despite a delocalization length of $v/\omega \sim 0.4$ μm. Figures 2(f) and 2(g) show the vibrational images on logarithmic scale and over a larger field of view in order to exhibit the "dipole tails." Moving the beam 20 Å from the molecule causes the intensity to drop by about four orders of magnitude.

V. DISCUSSION

The CO example demonstrates that, at high spatial resolution, the long-ranged nature of dipole scattering is counterbalanced by its small amplitude: For small detector angles
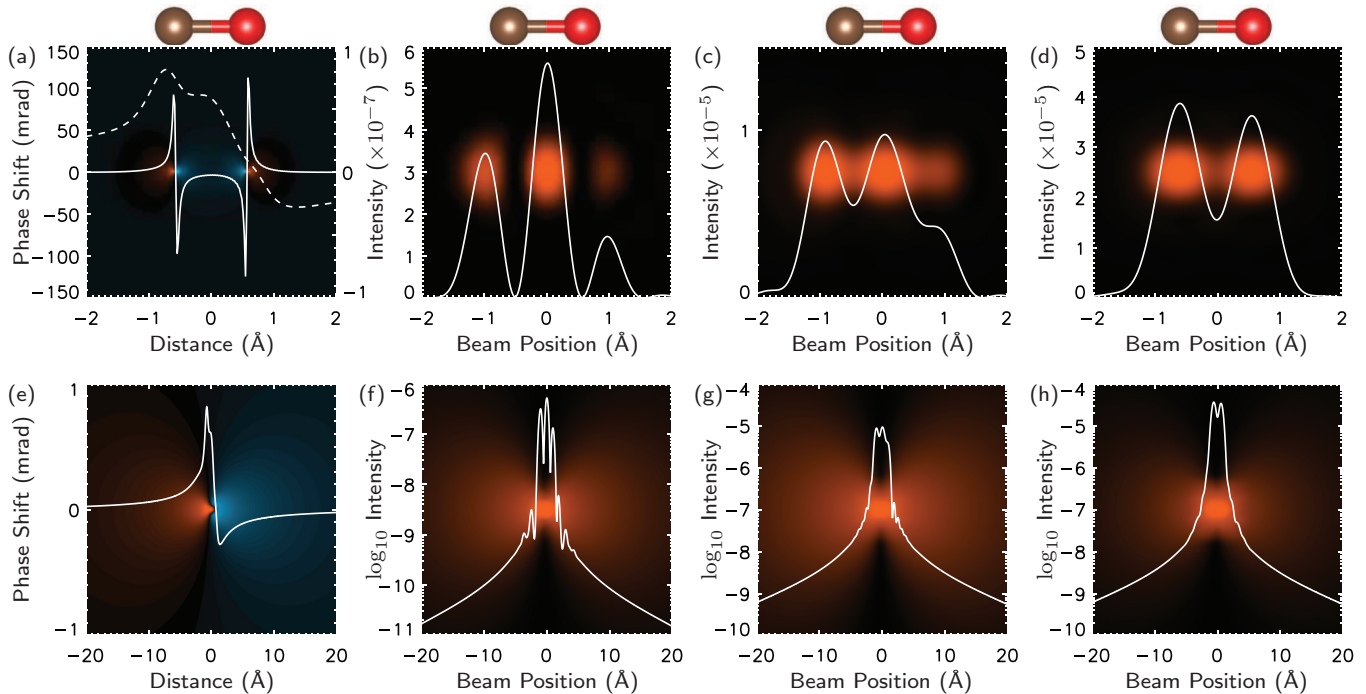
FIG. 2. (Color online) Effect of dipole scattering on vibrational EELS imaging of a CO molecule lying perpendicular to the electron beam (C on the left): (a) Impact potential for excitation of CO stretching mode (solid line, left ordinate) with dipole potential overlaid (dashed line, right ordinate); (b)–(d) vibrational EELS images for detector semiangles of 5, 30, and 80 mrad; (e) dipole potential shown over a larger field of view; (f)–(h) vibrational EELS images shown on a logarithmic scale and over a larger field of view. Beam parameters match Fig. 1.

its contribution is comparable to that of impact scattering, whereas for larger detector angles impact scattering dominates. While we do not claim that this must hold for absolutely all targets, the strength of the CO dynamic dipole is, however, representative of a fairly large class of molecules. In cases where the dipole scattering is even stronger, its effect could be circumvented by employing, for example, an annular detector that excludes the dipole scattering at low angles (although this would also diminish the desirable impact signal).

Note that this situation is complementary to HREELS investigations, which uses low-energy electrons in a reflection geometry, and where dipole scattering is often selected by employing a small acceptance angle [4]. In this context, it is interesting to recall a statement made over 30 years ago by Ibach and Mills: "In the impact scattering regime, the total excitation efficiency $(dS/d\Omega)$ increases as the electron [incident] energy increases. It thus would be most favorable to study large-angle inelastic electron scattering at [incident] energies substantially larger than that used in present generation [low-energy] experiments, if suitable spectrometers could be constructed" [4]. Indeed, our detailed calculations show that this idea is very favorable for achieving high spatial resolution.

It was noted earlier that only for a detector angle larger than the convergence angle is the image contrast in Figs. 1 and 2 intuitively interpretable in terms of the molecule's structure. We have also confirmed this behavior for other atomic structures, including solids and adsorbate molecules on surfaces (to be presented elsewhere). In addition to better interpretability, a larger detector has the benefit of a stronger

signal. Experimentally, on the other hand, larger detector angles do place greater demands on the spectrometer optics to achieve a given energy resolution, so that a compromise between interpretability and energy resolution is likely to be necessary in practice.

Returning to the general question of the implications of delocalization in the inelastic scattering of high-energy electrons, considerable insight can be gained by considering the form of the projected Møller potential. A useful interpretation of this potential is that it represents the interaction between the charge distributions of the scattering electron and the transitioning target. The scattering electron's charge distribution *oscillates* along the direction of motion with period $2\pi v/\omega$ due to the momentum change along the direction of motion (Fig. 3). The oscillation means that an electron passing the target at a closest distance $d \gg 2\pi v/\omega$ cannot interact appreciably with it [Fig. 3(a)]. On the other hand, if the closest approach satisfies $d \lesssim 2\pi v/\omega$, then portions of the scattering electron's positive and negative charges lie at appreciably different distances from the target and an interaction is possible [Fig. 3(b)]. Mathematically, the projected Møller potential can be written in the form

$$V_{\text{Møller}}(\mathbf{x}) = \frac{-e}{2\pi} \int d^2\mathbf{x}' \rho(\mathbf{x}') K_0\left(\frac{\omega}{v}|\mathbf{x} - \mathbf{x}'|\right), \qquad (4)$$

where ρ is the charge distribution of the transitioning target, K_0 is a modified Bessel function, bold symbols denote two-dimensional (2D) vectors, and $\mathbf{x}$ is the electron's position. This expression is exactly analogous to the well-known Yukawa potential describing short-ranged interactions between
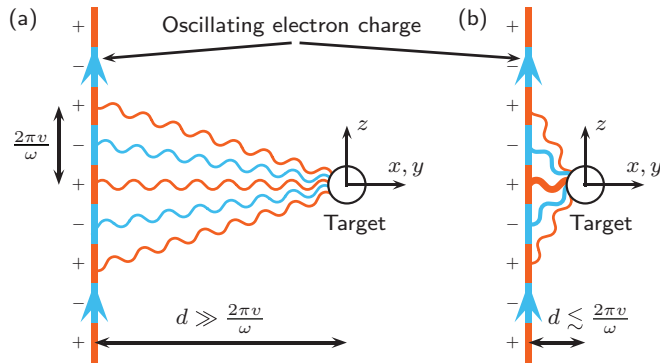
FIG. 3. (Color online) The physical origin of spatial localization in inelastic electron scattering. (a) If the distance d of closest approach to the target well exceeds the oscillation period $2\pi v/\omega$ of the incident electron's charge distribution then the Møller interaction cancels. (b) If the distance of closest approach is comparable to or smaller than $2\pi v/\omega$ then an interaction is possible.

nucleons. The modified Bessel function plays the role of a "2D Yukawa potential": At small distances it behaves as $-\ln|\mathbf{x}|$, while at large distances it behaves as $e^{-(\omega/v)|\mathbf{x}|}/\sqrt{\mathbf{x}}$, that is, exponentially damped, which cuts off the interaction. (As an interesting aside, recalling that in quantum field theory the Yukawa force is "carried" by particles with mass; here, by analogy, the carrier particles move in two dimensions with a mass $\hbar\omega/vc$.)

From the present discussion, it should be clear that the quantity v/ω represents an *upper* limit on the interaction distance, and that the interaction *can* be strictly more localized than v/ω if the charge distribution of the target permits. The H_2 example above, where there is an absence of a dipole field at large distances, is a case in point. Even when the transitioning target does produce a dipole field, if its effect is sufficiently weak then the interaction can still be effectively more localized than v/ω, as in the CO example above.

VI. CONCLUSIONS

In summary, we have determined that, while the effects of long-ranged dipole scattering and delocalization can be present in inelastic scattering of high-energy electrons from vibrational excitations, the scattering physics permits atomic spatial resolution nonetheless. These results motivate the development of high-spatial-resolution vibrational spectroscopy as a potentially extremely powerful and unique analytical technique in the physical sciences.

[1] O. L. Krivanek, T. C. Lovejoy, N. Dellby, and R. W. Carpenter, Microscopy **62**, 3 (2013).

[2] R. H. Ritchie and A. Howie, Philos. Mag. A **58**, 753 (1988).

[3] D. A. Muller and J. Silcox, Ultramicroscopy **59**, 195 (1995).

[4] H. Ibach and D. L. Mills, *Electron Energy Loss Spectroscopy and Surface Vibrations* (Academic Press, London, 1982).

[5] M. Bosman, V. J. Keast, J. L. García-Muñoz, A. J. D'Alfonso, S. D. Findlay, and L. J. Allen, Phys. Rev. Lett. **99**, 086102 (2007).

[6] K. Kimoto, T. Asaka, T. Nagai, M. Saito, Y. Matsui, and K. Ishizuka, Nature (London) **450**, 702 (2007).

[7] D. A. Muller, L. Fitting Kourkoutis, M. Murfitt, J. H. Song, H. Y. Hwang, J. Silcox, N. Dellby, and O. L. Krivanek, Science **319**, 1073 (2008).

[8] M. A. Chesters, in *Handbook of Vibrational Spectroscopy*, edited by J. M. Chalmers and P. Griffiths (John Wiley and Sons, New York, 2006), p. 830.

[9] G. Kresse and J. Furthmüller, Phys. Rev. B **54**, 11169 (1996).

[10] G. Kresse and D. Joubert, Phys. Rev. B **59**, 1758 (1999).

[11] K. Parlinski, Z.-Q. Li, and Y. Kawazoe, Phys. Rev. Lett. **78**, 4063 (1997).

[12] A. Togo, F. Oba, and I. Tanaka, Phys. Rev. B **78**, 134106 (2008).

[13] C. Dwyer, Ultramicroscopy **104**, 141 (2005).

[14] P. Rez, C. J. Humphreys, and M. J. Whelan, Philos. Mag. **35**, 81 (1977).

[15] H. Kohl and H. Rose, Adv. Imaging Electron Phys. **65**, 173 (1985).

[16] E. J. Kirkland, *Advanced Computing in Electron Microscopy*, 2nd ed. (Springer, New York, 2010).

[17] G. D. Dickenson, M. L. Niu, E. J. Salumbides, J. Komasa, K. S. E. Eikema, K. Pachucki, and W. Ubachs, Phys. Rev. Lett. **110**, 193601 (2013).

[18] H. L. Xin, Y. Zhu, and D. A. Muller, Microsc. Microanal. **18**, 720 (2012).

[19] M. P. Oxley, E. C. Cosgriff, and L. J. Allen, Phys. Rev. Lett. **94**, 203906 (2005).

[20] C. Dwyer, S. D. Findlay, and L. J. Allen, Phys. Rev. B **77**, 184107 (2008).

[21] P. A. Thiry, M. Liehr, J. J. Pireaux, and R. Caudano, Phys. Scr. **35**, 368 (1987).

[22] M. Schönnenbeck, D. Cappus, J. Klinkmann, H. J. Freund, L. G. M. Petterson, and P. S. Bagus, Surf. Sci. **347**, 337 (1996).

[23] R. D. Nelson, Jr., D. R. Lide, Jr., and A. A. Maryott, National Bureau of standards (U.S.) Technical Report No. 10, 1967 (unpublished).